Geophysical Prospecting, 1998, 46, 249–270

Viscoelastic effective rheologies for modelling wave propagation in porous media[1]

José M. Carcione[2]

Abstract

Biot's poroelastic differential equations are modified for including matrix–fluid interaction mechanisms. The description is phenomenological and assumes a solid–fluid relaxation function coupling coefficient. The model satisfies basic physical properties such as, for instance, that P-wave velocities at low frequencies are lower than those predicted by Biot's theory.

In many cases, the results obtained with the Biot (two-phase) modelling are equal to those obtained with single-phase *elastic* modelling, mainly at seismic frequencies. However, a correct equivalence is obtained with a *viscoelastic* rheology, which requires one relaxation peak for each Biot (P and S) mechanism. The standard viscoelastic model, which generalizes compressibility and shear modulus to relaxation functions, is not appropriate for modelling the Biot complex moduli, since Biot's attenuation is of a kinetic nature (i.e. it is not related to bulk deformations). The problem is solved by associating relaxation functions with each wave modulus.

The equivalence between the two modelling approaches is investigated for a homogeneous water-filled sandstone and a periodically layered poroelastic medium, alternately filled with gas and water. The simulations indicate that, in the homogeneous case, particle velocities in the solid skeleton, caused by a source applied to the matrix, are equivalent to viscoelastic particle velocities. In a finely layered medium, viscoelastic modelling is not, in principle, equivalent to porous modelling, due to substantial mode conversion from fast wave to slow static mode. However, this effect, caused by local fluid-flow motion, can be simulated by including an additional relaxation mechanism similar to the squirt-flow.

Introduction

Biot's theory of dynamic poroelasticity (Biot 1962) successfully describes the wave propagation properties of synthetic porous media such as sintered glass beads. In natural porous media such as sandstone, discrepancies between Biot's theory and measurements are due to complex pore shapes that are not present in simple synthetic

[1] Received December 1996, revision accepted October 1997.
[2] Osservatorio Geofisico Sperimentale, PO Box 2011, Opicina, 34016 Trieste, Italy.

© 1998 European Association of Geoscientists & Engineers

media (Gist 1994). This complexity gives rise to a variety of matrix–fluid interactions which contribute to the attenuation of the different wave modes. The most important interaction is the squirt-flow mechanism, which explains the energy losses and levels of velocity dispersion at sonic and ultrasonic frequencies (Dvorkin, Nolen-Hoeksema and Nur 1994). In this paper, the different matrix–fluid attenuation mechanisms are introduced into Biot's theory by substituting the fluid–solid coupling modulus by a time-dependent relaxation function based on the standard linear solid model. The introduction of memory variables for avoiding the time convolutions yields a set of first-order differential equations for dynamic poroviscoelasticity.

It has been suggested that the value of poroelastic wave modelling is unclear without comparison of its results with the corresponding simulations based on single-phase modelling (Gurevich 1996). This is particularly important at the seismic range where poroelastic effects are relatively small. However, Norris (1993) and Gurevich and Lopatnikov (1995) have shown that attenuation levels and velocity-dispersion measurements can be explained by the combined effects of layering and energy transfer between wave modes. For instance, if the fluid compressibility varies significantly from point to point, diffusion of pore fluid between different regions constitutes a mechanism that can be important at seismic frequencies. Modelling the anelastic properties of poroviscoelastic waves with a single-phase rheological equation is performed by assigning relaxation functions to each wave mode and fitting the attenuation factors and phase-velocity dispersion curves of the fast waves.

Biot's poroviscoelastic differential equations (Biot 1962) have the form $\dot{\mathbf{v}} = \mathbf{M}\mathbf{v}$, where $\mathbf{v}$ is the wavefield vector and $\mathbf{M}$ is the propagation matrix (the dot denotes differentiation with respect to time). All the eigenvalues of $\mathbf{M}$ have a negative real part. While the eigenvalues of the fast wave have a small real part, the eigenvalues of the slow wave (in the diffusive regime) have a large real part. The presence of this diffusive mode makes the differential equations stiff, and then seismic and sonic modelling are unstable when using explicit time-integration methods. In both cases, the Biot peaks (i.e. the presence of the diffusive mode) make the problem stiff; in the seismic case, the squirt-flow mechanism also contributes to the stiffness of the differential equations. The use of an A-stable Crank-Nicholson scheme provides a reasonable solution to the problem in terms of efficiency and accuracy (Carcione and Quiroga-Goode 1995).

This work compares two-phase and single-phase modelling results in homogeneous and periodic layered media, at both seismic and sonic frequencies. Moreover, the problem of the gas–water contact studied by Dutta and Ode (1983) is solved. The simulations evaluate the equivalence between the Biot (i.e. porous) and the viscoelastic modelling. In addition, a valid implementation of the squirt-flow mechanism into Biot's equations requires certain physical properties to be satisfied. This is investigated in the frequency domain and the corresponding differential equations are obtained.

Poroviscoelastic equations of motion

The constitutive equations for an inhomogeneous, isotropic poroelastic medium under

plane strain conditions are given by (Biot and Willis 1957; Biot 1962)

$$\tau_{xx,t} = Ev_{x,x} + (E - 2\mu)v_{z,z} + \alpha M\epsilon + s_x, \tag{1}$$

$$\tau_{zz,t} = (E - 2\mu)v_{x,x} + Ev_{z,z} + \alpha M\epsilon + s_z, \tag{2}$$

$$\tau_{xz,t} = \mu(v_{x,z} + v_{z,x}) + s_{xz}, \tag{3}$$

$$p_{,t} = -M\epsilon + s_f, \tag{4}$$

$$\epsilon = \alpha(v_{x,x} + v_{z,z}) + q_{x,x} + q_{z,z}, \tag{5}$$

where τ_{xx}, τ_{zz} and τ_{xz} are the total stress components, p is the fluid pressure, v and q are the solid and fluid (relative to the solid) particle velocities, and s_x, s_z, s_{xz} and s_f are the external sources of stress, for the solid and the fluid, respectively. The subscript '$,x$' denotes $\partial/\partial x$.

The elastic coefficients are given by

$$E = K_m + \frac{4}{3}\mu, \tag{6}$$

$$M = \frac{K_s^2}{D - K_m}, \tag{7}$$

$$D = K_s[1 + \phi(K_s K_f^{-1} - 1)], \tag{8}$$

$$\alpha = 1 - \frac{K_m}{K_s}, \tag{9}$$

where K_m, K_s and K_f are the bulk moduli of the drained matrix, solid and fluid, respectively, ϕ is the porosity and μ is the shear modulus of the drained (and saturated) matrix. The stiffness E is the P-wave modulus of the dry skeleton, M is the coupling modulus between the solid and the fluid, and α is the poroelastic coefficient of effective stress.

Viscoelasticity is introduced into Biot's poroelastic equations (Biot 1962) for modelling a variety of dissipation mechanisms related to the skeleton–fluid interaction. One of these mechanisms is the squirt-flow (Biot 1962), by which a force applied to the area of contact between two grains produces a displacement of the surrounding fluid in and out of this area. Since the fluid is viscous, the motion is not instantaneous and energy dissipation occurs. Skeleton–fluid mechanisms are modelled by generalizing the coupling modulus M to a time-dependent relaxation function. We assume that E and μ are frequently independent.

The term $M\epsilon$ in (1), (2) and (4) is replaced by $\psi \star \epsilon_{,t}$, where

$$\psi(t) = M\left(1 + \frac{1}{L}\sum_{l=1}^{L}\varphi_l\right)^{-1}\left[1 + \frac{1}{L}\sum_{l=1}^{L}\varphi_l \exp(-t/\tau_{\sigma l})\right]\mathrm{H}(t), \tag{10}$$

where H(t) denotes the Heaviside function,

$$\varphi_l = \frac{\tau_{\epsilon l}}{\tau_{\sigma l}} - 1, \tag{11}$$

and $\tau_{\epsilon l}$ and $\tau_{\sigma l}$ denote sets of relaxation times. Equation (10) corresponds to a parallel connection of standard linear solid elements. For high frequencies ($t = 0^+$), $\psi = M$. As in the single-phase viscoelastic case (Carcione 1995), we introduce memory variables in order to avoid the time convolutions.

The poroviscoelastic equations of motion are:

(i) Biot–Newton's dynamic equations (Biot 1962):

$$\tau_{xx,x} + \tau_{xz,z} = \rho v_{x,t} + \rho_f q_{x,t}, \tag{12}$$

$$\tau_{xz,x} + \tau_{zz,z} = \rho v_{z,t} + \rho_f q_{z,t}, \tag{13}$$

where

$$\rho = (1 - \phi)\rho_s + \phi\rho_f$$

is the composite density, and ρ_s and ρ_f are the solid and fluid densities, respectively.

(ii) Dynamic Darcy's law:

$$-p_{,x} = \rho_f v_{x,t} + m q_{x,t} + \frac{\eta}{\kappa} q_x, \tag{14}$$

$$-p_{,z} = \rho_f v_{z,t} + m q_{z,t} + \frac{\eta}{\kappa} q_z, \tag{15}$$

where $m = T\rho_f/\phi$, T denotes the tortuosity, η is the fluid viscosity and κ is the permeability of the medium.

(iii) Constitutive equations:

$$\tau_{xx,t} = E v_{x,x} + (E - 2\mu) v_{z,z} + \alpha\left(M\epsilon + \sum_{l=1}^{L} e_l\right) + s_x, \tag{16}$$

$$\tau_{zz,t} = (E - 2\mu) v_{x,x} + E v_{z,z} + \alpha\left(M\epsilon + \sum_{l=1}^{L} e_l\right) + s_z, \tag{17}$$

$$\tau_{xz,t} = N(v_{x,z} + v_{z,x}) + s_{xz}, \tag{18}$$

$$p_{,t} = -\left(M\epsilon + \sum_{l=1}^{L} e_l\right) + s_f, \tag{19}$$

where e_l, $l = 1, \ldots, L$ are the memory variables.

For application of the source, consider three main cases (Carcione and Quiroga-Goode 1996):

1 Frame source: $s_f = 0$, and the various combinations of s_x, s_z and s_{xz} giving a

horizontal force, a vertical force, an explosive source and a purely shear source, all applied to the skeleton.
2 Fluid volume injection: $s_x = s_z = \phi s_f$ and $s_{xz} = 0$.
3 Bulk source: this case assumes that the energy is partitioned between the two phases and that the radiation pattern is isotropic, $s_x = s_z = s_f$ and $s_{xz} = 0$.

(iv) Memory variable equations:

$$e_{l,t} = -\frac{1}{\tau_{\sigma l}}\left[M\left(L + \sum_{m=1}^{L}\varphi_m\right)^{-1}\varphi_l\epsilon + e_l\right], \tag{20}$$

for $l = 1, \ldots, L$.

Phase velocity and attenuation for porous media

The calculation of the phase velocity and attenuation factor requires a Fourier transformation of the constitutive equations to the frequency domain, implying the following substitution

$$M \rightarrow M_c$$

where

$$M_c = M\left(L + \sum_{l=1}^{L}\varphi_l\right)^{-1}\sum_{l=1}^{L}\frac{1 + i\omega\tau_{el}}{1 + i\omega\tau_{\sigma l}}, \tag{21}$$

where ω denotes the angular frequency. The relaxation times can be expressed in terms of a Q-factor, Q_{0l}, and a reference frequency, f_{0l}, as

$$\tau_{el} = \frac{1}{2\pi f_{0l}Q_{0l}}\left[\sqrt{Q_{0l}^2 + 1} + 1\right] \tag{22}$$

and

$$\tau_{\sigma l} = \frac{1}{2\pi f_{0l}Q_{0l}}\left[\sqrt{Q_{0l}^2 + 1} - 1\right]. \tag{23}$$

The velocities of the fast (+ sign) and slow (− sign) compressional waves and shear wave are given by (see, for example, Carcione 1996)

$$V_{P\pm}^2 = \frac{A \pm \sqrt{A^2 - 4M_cE\rho_c\bar{\rho}}}{2\rho_c\bar{\rho}} \tag{24}$$

and

$$V_S^2 = \frac{N}{\rho_c}, \tag{25}$$

where

$$A = M_c(\rho - 2\alpha\rho_f) + \overline{\rho}(E + \alpha^2 M_c),$$

$$\rho_c = \rho - \rho_f^2/\overline{\rho},$$

and

$$\overline{\rho} = \frac{T}{\phi}\rho_f - \frac{\mathrm{i}}{2\pi f}\frac{\eta}{\kappa},$$

where f denotes the frequency and $\mathrm{i} = \sqrt{-1}$. Similar expressions for the complex velocities in an isotropic Biot's medium are given by, for instance, Dutta and Ode (1983). The difference resides in the fact that (24) is explicitly dependent on the complex viscoelastic quantity M_c. Note that V_S does not depend on M_c and therefore skeleton–fluid interactions do not affect the shear wave.

The phase velocity c is equal to the angular frequency $\omega = 2\pi f$ divided by the real wavenumber. Then

$$c_{P\pm} = \left[\mathrm{Re}\left(\frac{1}{V_{P\pm}}\right)\right]^{-1}, \quad c_S = \left[\mathrm{Re}\left(\frac{1}{V_S}\right)\right]^{-1}, \tag{26}$$

where Re denotes the real part. Following Dutta and Ode (1983), we define the attenuation coeficients as

$$\alpha_{P\pm} = 17.372\pi\frac{\mathrm{Im}(V_{P\pm})}{\mathrm{Re}(V_{P\pm})}, \quad \alpha_S = 17.372\pi\frac{\mathrm{Im}(V_S)}{\mathrm{Re}(V_S)}, \tag{27}$$

where Im denotes the imaginary part.

Equivalent viscoelastic equations of motion

The attenuation in Biot's poroelastic equations is not caused by bulk viscoelasticity (through the stress–strain relations), and therefore the standard viscoelastic model, which generalizes compressibility and shear modulus to relaxation functions, is not appropriate to describe the Biot complex moduli. Instead, we try to match directly the compressional and shear attenuation and velocity dispersion by using relaxation functions associated with each wave mode. Since, within the present extension of Biot's theory, the squirt-flow mechanism does not affect the shear wave, this is described by one set of relaxation times. The equations are similar to those obtained by Carcione (1995), but contain an additional memory variable per set of relaxation times.

The two-dimensional velocity–stress equations for propagation in the (x, y)-plane, assigning one relaxation mechanism to each wave mode, can be expressed as:

(i) Newton's equations:

$$\sigma_{xx,x} + \sigma_{xz,z} = \rho v_{x,t} + f_x, \tag{28}$$

$$\sigma_{xz,x} + \sigma_{zz,z} = \rho v_{z,t} + f_z, \tag{29}$$

where v_x, and v_z are the particle velocities, σ_{xx}, σ_{zz} and σ_{xz} are the stress components, ρ is the density and f_x and f_z are the body forces.

(ii) Constitutive equations:

$$\sigma_{xx,t} = \rho c_{\mathrm{P}\infty}^2 (v_{x,x} + v_{z,z}) - 2\rho c_{\mathrm{S}\infty}^2 v_{z,z} + \sum_{l=1}^{L} \epsilon_{1l} - 2\epsilon_2 + s_x, \tag{30}$$

$$\sigma_{zz,t} = \rho c_{\mathrm{P}\infty}^2 (v_{x,x} + v_{z,z}) - 2\rho c_{\mathrm{S}\infty}^2 v_{x,x} + \sum_{l=1}^{L} \epsilon_{1l} - 2\epsilon_3 + s_z, \tag{31}$$

$$\sigma_{xz,t} = \rho c_{\mathrm{S}\infty}^2 (v_{x,z} + v_{z,x}) + \epsilon_4 + s_{xz}, \tag{32}$$

where

$$c_{\mathrm{P}\infty}^2 = \frac{c_{\mathrm{P}0}^2}{L} \sum_{l=1}^{L} \frac{\tau_{+l}^{(1)}}{\tau_{-l}^{(1)}} \quad \text{and} \quad c_{\mathrm{S}\infty}^2 = c_{\mathrm{S}0}^2 \frac{\tau_+^{(2)}}{\tau_-^{(2)}} \tag{33}$$

are the squared high-frequency compressional and shear velocities, respectively, and s_x, s_z and s_{xz} are external forces equivalent to the sources used in the porous case (see equations (1)–(3)). Moreover, the memory variables ϵ_{1l} and ϵ_j, $j = 2, \ldots, 4$ satisfy the following equations:

(iii) Memory variable equations:

$$\epsilon_{1l,t} = \phi_{1l}(v_{x,x} + v_{z,z}) - \frac{\epsilon_{1l}}{\tau_{-l}^{(1)}}, \quad l = 1, \ldots, L, \tag{34}$$

$$\epsilon_{2,t} = \phi_2 v_{z,z} - \frac{\epsilon_2}{\tau_-^{(2)}}, \tag{35}$$

$$\epsilon_{3,t} = \phi_2 v_{x,x} - \frac{\epsilon_3}{\tau_-^{(2)}}, \tag{36}$$

$$\epsilon_{4,t} = \phi_2 (v_{x,z} + v_{z,x}) - \frac{\epsilon_4}{\tau_-^{(2)}}, \tag{37}$$

where

$$\phi_{1l} = \frac{\rho c_{\mathrm{P}0}^2}{L \tau_{-l}^{(1)}} \left(1 - \frac{\tau_{+l}^{(1)}}{\tau_{-l}^{(1)}}\right), \quad \phi_2 = \frac{\rho c_{\mathrm{S}0}^2}{\tau_-^{(2)}} \left(1 - \frac{\tau_+^{(2)}}{\tau_-^{(2)}}\right). \tag{38}$$

Phase velocity and attenuation for viscoelastic media

The transformation to the frequency domain of the viscoelastic constitutive equations yields the complex velocities. As mentioned in the previous section, a set of relaxation mechanisms was associated with the compressional wave and one relaxation

mechanism was associated with the shear wave. The respective dimensionless complex moduli can be expressed as

$$M_1(f) = \frac{1}{L}\sum_{l=1}^{L}\frac{1+\mathrm{i}2\pi f\tau_{+l}^{(1)}}{1+\mathrm{i}2\pi f\tau_{-l}^{(1)}} \tag{39}$$

and

$$M_2(f) = \frac{1+\mathrm{i}2\pi f\tau_{+}^{(2)}}{1+\mathrm{i}2\pi f\tau_{-}^{(2)}}, \tag{40}$$

where the relaxation times can be related to the more physical parameters Q_{1l}, f_{1l}, Q_2 and f_2 by the following formulae:

$$\tau_{\pm l}^{(1)} = \frac{1}{2\pi f_{1l}Q_{1l}}\left[\sqrt{Q_{1l}^2+1}\pm 1\right] \tag{41}$$

and

$$\tau_{\pm}^{(2)} = \frac{1}{2\pi f_2 Q_2}\left[\sqrt{Q_2^2+1}\pm 1\right]. \tag{42}$$

The quality factor associated with the compressional wave is equal to the real part of M_1 divided by its imaginary part. For instance, in the case of two dissipation mechanisms, Q_{11} and Q_{12} are related to the quality factors of the squirt-flow and the Biot mechanisms with maximum attenuation at the frequencies f_{11} and f_{12}, respectively.

The complex velocities of the P- and S-waves in 2D viscoelastic media are (for example Carcione 1995)

$$\bar{V}_{\mathrm{P}}^2 = c_{\mathrm{P}0}^2 M_1 \tag{43}$$

and

$$\bar{V}_{\mathrm{S}}^2 = c_{\mathrm{S}0}^2 M_2 \tag{44}$$

where $c_{\mathrm{P}0}$ and $c_{\mathrm{S}0}$ are the Biot low-frequency phase velocities of the fast compressional and shear waves, respectively. The viscoelastic phase velocities and attenuation factors can be obtained similarly from (26) and (27).

Effective viscoelastic medium

A homogeneous porous medium can be modelled by a single-phase viscoelastic medium. As will be seen below, only one relaxation mechanism for each viscoelastic modulus is enough to fit the moduli of the porous medium.

We consider the same media as analysed by Dutta and Ode (1983), who computed the reflection coefficients for a gas–water contact. The material properties of the single constituents and saturated porous medium are given in Tables 1 and 2, respectively. Table 2 gives the relaxed ($\omega = 0$) and unrelaxed ($\omega = \infty$) phase velocities, and the attenuation factors at the central frequency of the Biot peak. Phase velocities and

Table 1. Material properties of the single constituents.

Solid	bulk modulus, K_s	35 GPa
	density, ρ_s	2650 kg/m^3
Matrix	bulk modulus, K_m	1.7 GPa
	shear modulus, N	1.855 GPa
	porosity, ϕ	0.3
	permeability, κ	1 D
	tortuosity, T	1
Gas	bulk modulus, K_g	0.022 GPa
	density, ρ_g	100 kg/m^3
	viscosity, η_g	0.015 cP
Water	bulk modulus, K_w	2.4 GPa
	density, ρ_w	1000 kg/m^3
	viscosity, η_w	1 cP

Table 2. Properties of the saturated rock: Biot's model.

	Water-filled	Gas-filled
ρ	2155 kg/m^3	1885 kg/m^3
$c_{P+}(0)$	2205 m/s	1500 m/s
$c_{P+}(\infty)$	2234 m/s	1506 m/s
$c_S(0)$	928 m/s	992 m/s
$c_S(\infty)$	1000 m/s	1000 m/s
$f_B(P+)$	67.54 kHz	8.07 kHz
$f_B(S)$	51.71 kHz	7.23 kHz
$\alpha_{P+}(f_B)$	0.356 dB	0.116 dB
$\alpha_S(f_B)$	2.044 dB	0.219 dB

Table 3. Properties of the equivalent viscoelastic media: Biot's model.

Pore fluid	c_{P0} (m/s)	c_{S0} (m/s)	ρ (kg/m^3)	f_1 (kHz)	f_2 (kHz)	Q_1	Q_2
Gas	1500	992	1885	8.07	7.23	119	125
Water	2205	928	2155	67.54	51.71	38.7	13.3

attenuations are shown by Dutta and Ode (1983), together with the reflection and transmission coefficients.

The properties of the equivalent viscoelastic media are shown in Table 3, where $\rho = (1-\phi)\rho_s + \phi\rho_f$ is the composite density. The squirt-flow mechanism is incorporated into the dynamic poroelasticity model by assuming $L = 1$ and $Q_0 = 10$ in (21), (22) and

Table 4. Properties of the saturated rock: BISF model.

	Water-filled	Gas-filled
ρ	2155 kg/m^3	1855 kg/m^3
$c_{P+}(0)$	2081 m/s	1498 m/s
$c_{P+}(\infty)$	2234 m/s	1506 m/s
$f_{SQ}(P+)$	3.22 kHz	7.80 kHz
$\alpha_{P+}(f_{SQ})$	1.597 dB	0.118 dB

(23). Following Dvorkin *et al.* (1994), we consider that, as the viscosity of the pore fluid decreases, the attenuation peak of the squirt-flow mechanism shifts towards higher frequencies. We assume $f_0 = 3$ kHz for water and $f_0 = 40$ kHz for gas. Table 4 gives the properties of the porous medium including this mechanism. The effect is to increase the attenuation level of the compressional wave in the sonic range and decrease the relaxed velocity. The S-wave is unaffected by the presence of the mechanism. The frequency f_{SQ} corresponds to the maximum attenuation. The properties of the equivalent viscoelastic media are shown in Table 5. Two relaxation mechanisms were used to fit the viscoelastic features of the compressional wave.

Figure 1 shows the attenuation factors as a function of frequency for gas and water pore fluids, where (a) corresponds to the Biot theory and (b) to the BISF (BIot plus Squirt-Flow) theory. The continuous line refers to the porous case and the dot to the single-phase viscoelastic theory. It can be shown that the attenuation associated with Biot's (Biot and Willis 1957) dilatational modulus,

$$\rho\left(\bar{V}_{P+}^2 - \frac{4}{3}\bar{V}_S^2\right),$$

is negative. In fact, Biot's attenuation is not of a viscoelastic nature, i.e. it is not associated with bulk deformations, and therefore the negative value has no physical meaning.

Figure 2 shows the P-wave phase velocities as functions of frequency for gas and water, with (a) and (b) illustrating the poroelastic and poroviscoelastic cases, respectively. The attenuations and phase velocities for the shear wave are shown in Fig. 3. Note that the shear-wave attenuation is higher than the poroviscoelastic

Table 5. Properties of the equivalent viscoelastic media: BISF model.

Pore fluid	c_{P0} (m/s)	c_{S0} (m/s)	ρ (kg/m^3)	f_1 (kHz)	f_2 (kHz)	Q_1	Q_2
Gas	1498	992	1885	0.28	7.23	330	125
				7.8		120	
Water	2081	928	2155	67.54	51.71	34	13.3
				3		9.2	

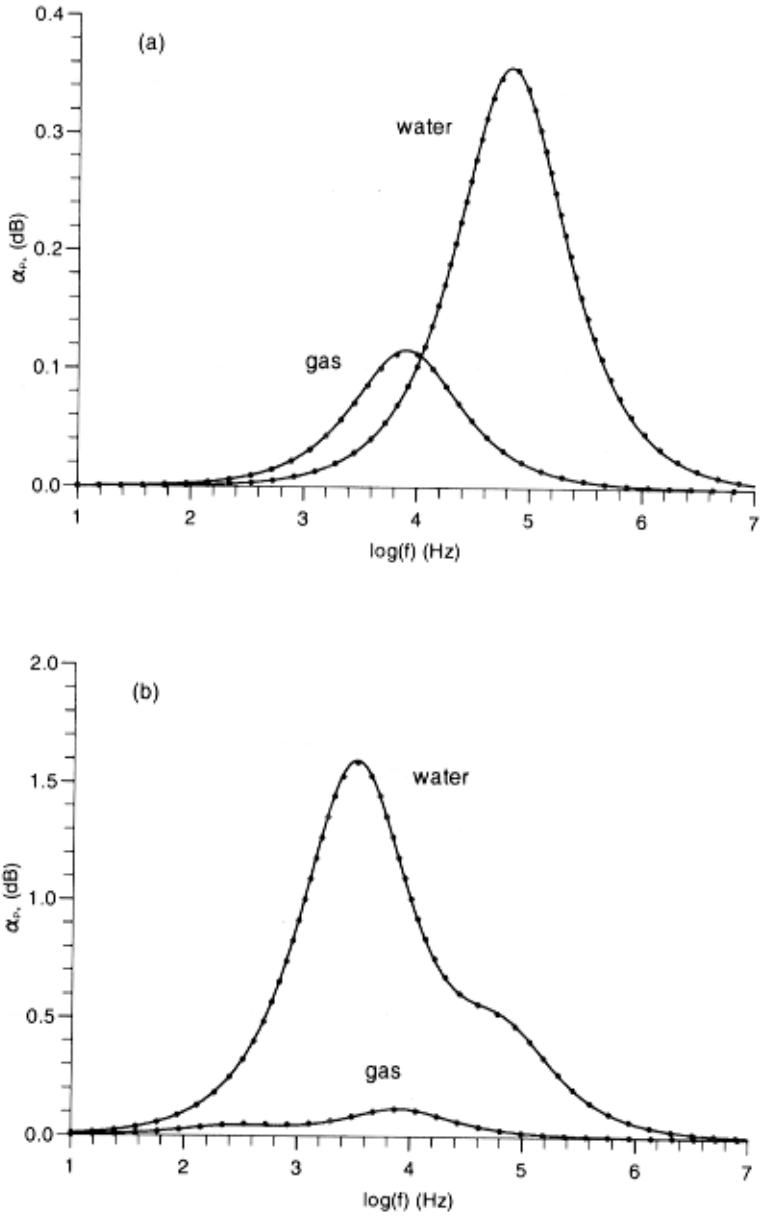

Figure 1. P_+-wave attenuation factors for water- and gas-saturated sandstone; (a) corresponds to Biot's theory and (b) to the combined Biot/squirt-flow (BISF) model. The continuous line corresponds to the porous medium solution, whose parameters are listed in Tables 2 and 4, and the dots to the viscoelastic equivalent media, whose parameters are given in Tables 3 (Biot) and 5 (BISF).

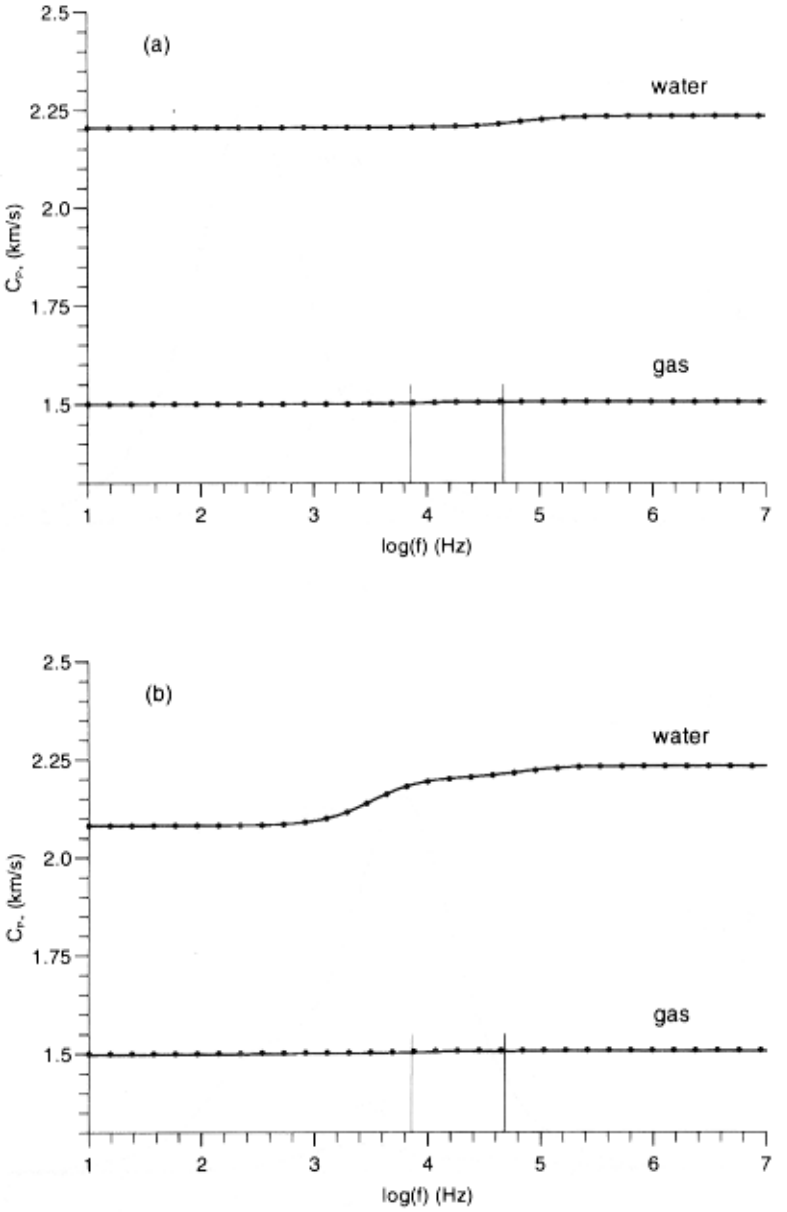

Figure 2. P_+-wave phase velocities for water- and gas-saturated sandstone; (a) corresponds to Biot's theory and (b) to the combined Biot/squirt-flow (BISF) model. The continuous line corresponds to the porous medium solution, whose parameters are listed in Tables 2 and 4, and the dots to the viscoelastic equivalent media, whose parameters are given in Tables 3 (Biot) and 5 (BISF). The vertical lines are the frequency limit for the validity of the low-frequency Biot's theory, $f_B = \eta\phi/(2\pi T \rho_f \kappa)$.

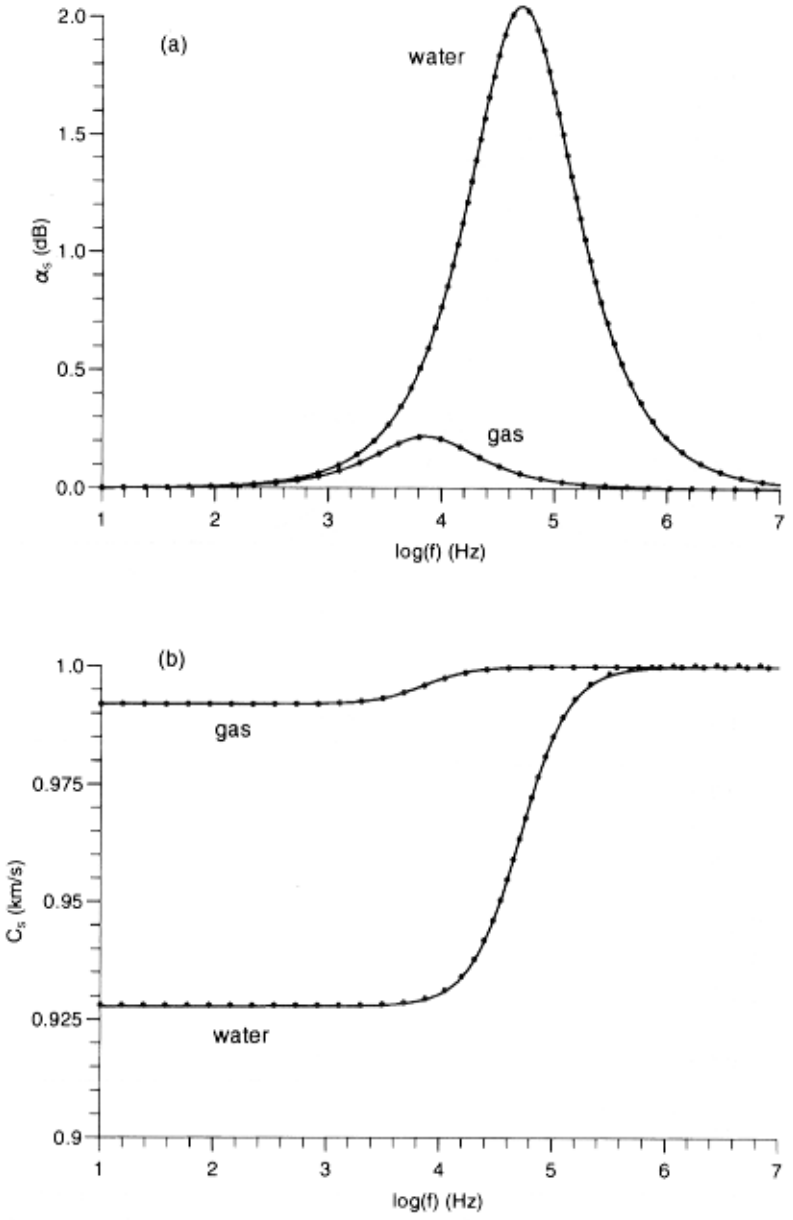

Figure 3. S-wave attenuation factors (a) and phase velocities (b) for water- and gas-saturated sandstone. The continuous line corresponds to the porous medium solution, whose parameters are listed in Tables 2 and 4, and the dots to the viscoelastic equivalent media, whose parameters are given in Tables 3 (Biot) and 5(BISF).

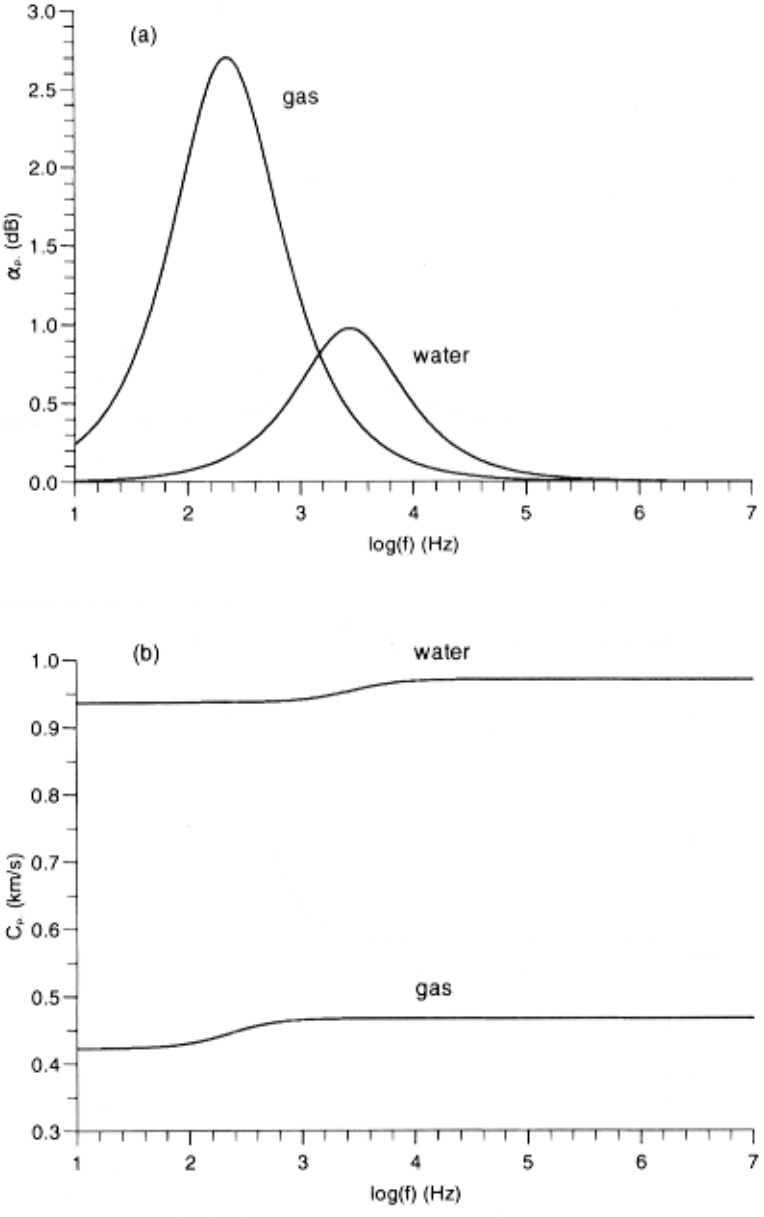

Figure 4. P_--wave attenuation factors (a) and phase velocities (b) for water- and gas-saturated sandstone. The curves correspond to the BISF model with $\eta = 0$.

compressional-wave attenuation (see Fig. 1b). The properties of the slow wave for $\eta = 0$ are illustrated in Fig. 4; the presence of the squirt-flow mechanism yields a relaxation peak near the exploration frequency band for gas-saturated sandstone. This behaviour is quite unexpected since, in the fast-wave case, the squirt-flow mechanism for gas peaks at a higher frequency than the corresponding mechanism in the water-saturated sandstone.

Simulations

The simulations are carried out in the seismic and sonic bands. The numerical meshes have 231×231 gridpoints, with a grid spacing of 5 m and 5 cm, respectively, and the source is dilatational ($s_x = s_z$ applied to the matrix) with central frequencies of 23 Hz and 2300 Hz, respectively. Both the viscoelastic and poroviscoelastic algorithms use time steps of 0.25×10^{-3} s and 0.25×10^{-5} s in the seismic and sonic cases, respectively.

The first simulation refers to Tables 2 and 3, and compares viscoelastic (single-phase) and poroelastic v_z snapshots in water-saturated sandstone. Figure 5 shows the snapshots at 2.7 s. As can be appreciated, both simulations are equivalent with the difference being less than 1 per cent.

Let us assume sonic frequencies, the presence of the squirt-flow mechanism and $\eta = 0$. In this case, the slow wave is a propagation mode whose properties are illustrated in Fig. 4. Poroviscoelastic snapshots computed at 2.7×10^{-3} s for water are illustrated in Fig. 6, where the outer (inner) front corresponds to the P_+ (P_-)-wave. The lower snapshot corresponds to a purely poroelastic rheology, i.e. no squirt-flow mechanism. In this case, the source central frequency is equal to 2100 Hz. At this frequency the attenuation factor of the P_+-wave is 1.6 dB which corresponds to a Q-factor of nearly 17. On the other hand, the P_--wave attenuation level at that frequency is 0.94 dB or a Q-factor equal to 30. This is the reason why the outer front is more attenuated by the squirt-flow mechanism than the slow wave.

In the next simulations, gridpoint 1 to gridpoint 105 is a periodic layering of gas- and water-saturated sandstone, with a thickness of one gridpoint, i.e. 5 m. From gridpoint 105 to gridpoint 231, the medium is homogeneous and saturated with water. The source, in the seismic range, is applied at gridpoint 105. Figure 7 shows the viscoelastic and poroelastic snapshots. The amplitudes on the lower part are similar while the amplitudes on the upper part are weaker in the poroelastic case, due to conversion from fast wave to slow mode. A similar 1D numerical experiment, showing this phenomenon, was performed by Turgut and Yamamoto (1988) for finely layered marine sediments. As demonstrated by Norris (1993) and Gurevich and Lopatnikov (1995), the attenuation/dispersion pair corresponding to this effect has the form which is typical for relaxation phenomena. The physical reason behind this anelastic behaviour is the combined effect of layering and local flow of the pore fluid between individual layers. Hence, the effect can be simulated in single-phase viscoelastic modelling by incorporating an additional relaxation mechanism. This phenomenon may explain the low signal-to-noise ratio P-wave sections observed in

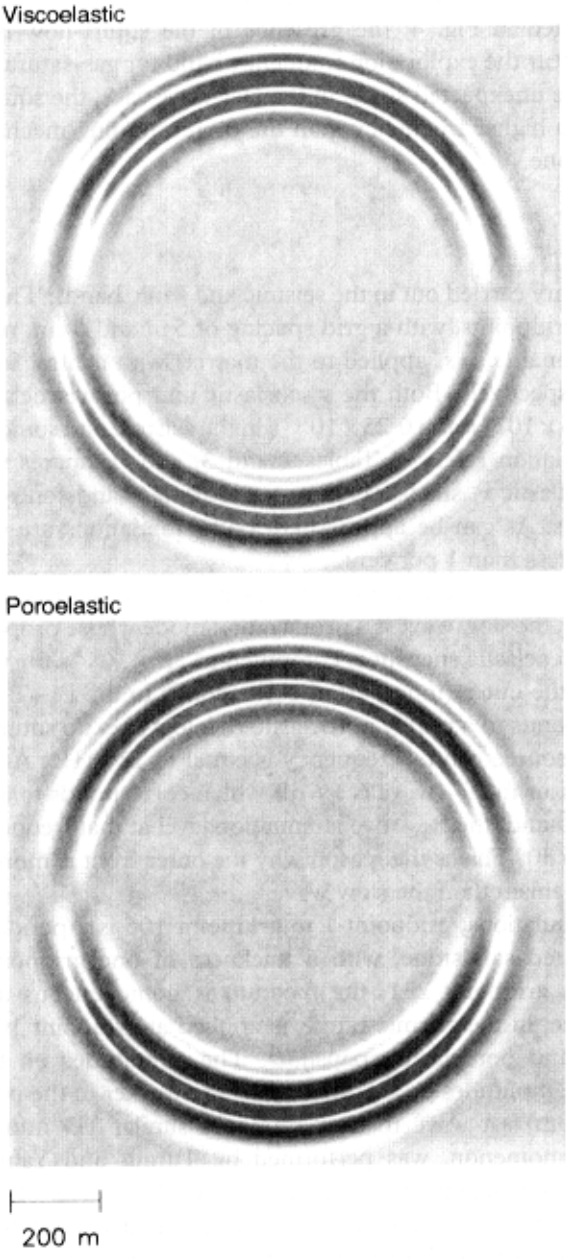

Figure 5. Viscoelastic (single-phase) and poroelastic (two-phase without squirt-flow) snapshots of the v_z particle-velocity component at 2.7 s. The medium is saturated with water and the source (in the seismic range) is dilatational, applied to the solid skeleton in the poroelastic case.

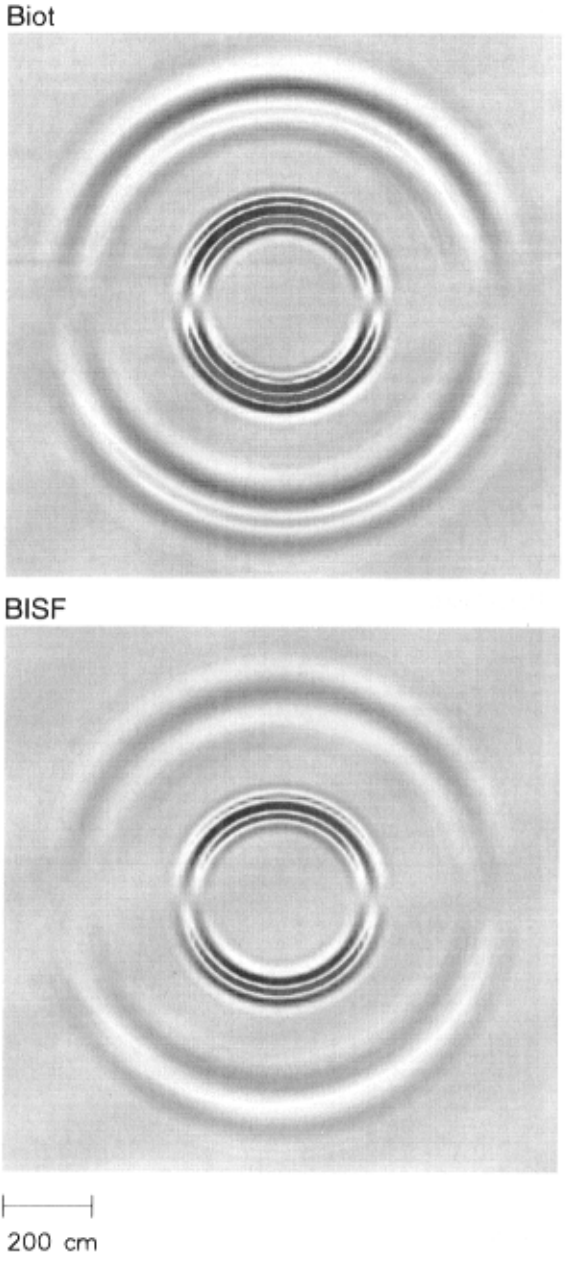

Figure 6. Poroviscoelastic and poroelastic snapshots computed at 2.7×10^{-3} s in a non-viscous ($\eta = 0$) water-saturated medium. The source (in the sonic range) is dilatational and is applied to the solid skeleton. The upper snapshot corresponds to a purely poroelastic rheology, i.e. no squirt-flow mechanism.

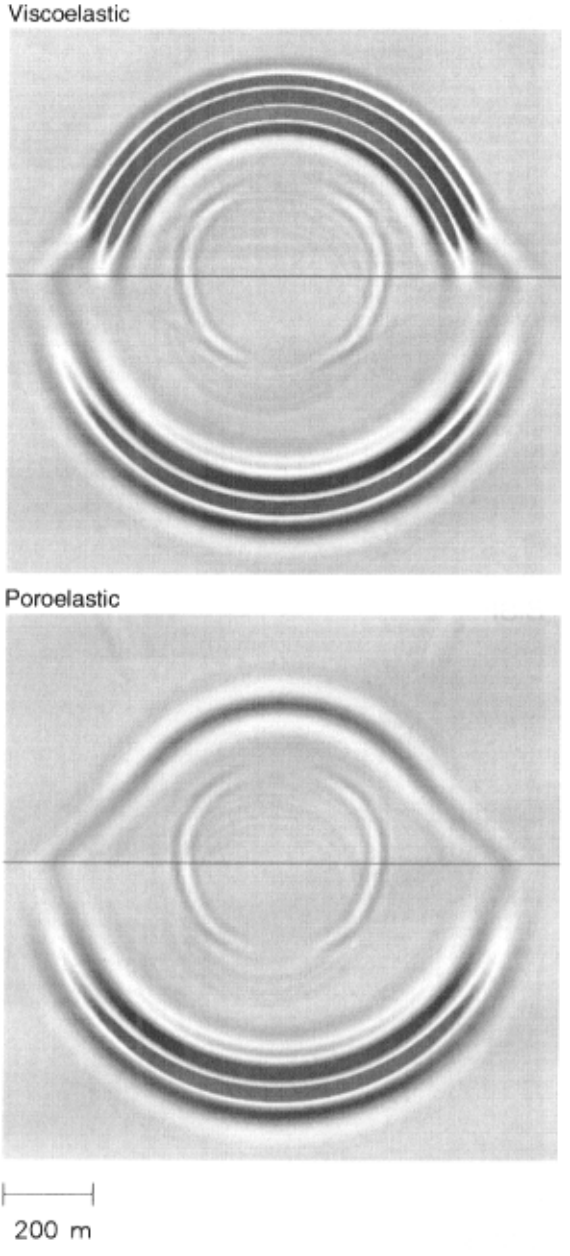

Figure 7. Viscoelastic (single-phase) and poroelastic (two-phase without squirt-flow) snapshots of the v_z particle-velocity component at 2.7 s. The upper medium is a periodic layering of gas- and water-saturated sandstone, and the lower medium is homogeneous water-saturated sandstone.

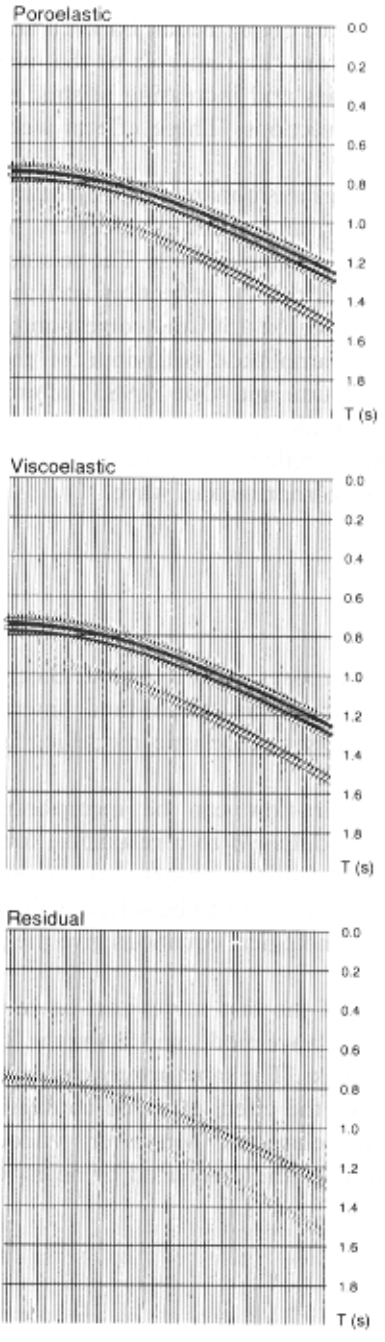

Figure 8. Viscoelastic (single-phase), poroelastic and residual v_z seismograms produced by a dilatational source of central frequency 23 Hz, located 520 m above a gas–water contact. The maximum offset is 1500 m.

some ocean-bottom seismic data (Kommedal, Barkved and Thomsen 1997). In fact, the presence of gas, leaked from the reservoir to the overburden, has the effect of both lowering seismic velocities and increasing seismic attenuation, producing low signal-to-noise ratio P-wave sections. These effects were not observed in S-wave sections.

Finally, we compute seismograms obtained with a dilatational source, located 520 m above the gas–water contract, and a line of receivers passing through the source location. In this case, the grid spacing is 10 m. The seismograms are shown in Fig. 8, where the upper hyperbola is the P_+ reflection and the lower event is the P_+-S conversion. A maximum offset of 1500 m, corresponding to an angle of 55°, is represented in Fig. 8. The amplitude behaviour of the reflected wave must be compared with Fig. 10 of Dutta and Ode (1983) after correction for geometrical spreading. The residual amplitudes, provided that the algorithms do not introduce any artefact, are due to a reduced reflection coefficient in the poroelastic case by mode conversion from fast to slow compressional wave.

Conclusions

The present work has two purposes: first, to extend Biot's theory in order to include relaxation mechanisms arising from grain–fluid interactions, and secondly, to investigate whether single-phase viscoelastic modelling is equivalent to poroelastic modelling.

Mechanisms like the squirt-flow can be incorporated into Biot's theory by generalizing the coupling modulus M to a relaxation function that yields M at the high-frequency limit. Introduction of memory variables avoids the time convolutions and gives a set of differential equations to be solved with Biot's differential equations. The so-called BISF phenomenological equations give the poroelastic equations at the high-frequency limit.

The anelastic properties of the fast waves can be modelled by using relaxation functions associated with each wave mode, and fitting the P and S relaxation peaks with corresponding viscoelastic peaks. The same approach can be used when the medium is highly inhomogeneous, since the effect of mode conversion from fast wave to slow mode shows a relaxation behaviour. Moreover, viscoelastic modelling is more convenient since the computer time is reduced by nearly 60 per cent compared with poroelastic modelling.

Acknowledgements

This work was supported in part by Norsk Hydro Bergen. Discussions with Boris Gurevich are gratefully acknowledged.

Appendix

Time-integration technique

The spatial derivatives are calculated with the Fourier method by using the fast Fourier transform (FFT). This approximation is infinitely accurate for band-limited periodic functions with cut-off spatial wavenumbers which are smaller than the cut-off wavenumbers of the mesh.

Since the presence of the slow compressional wave makes Biot's differential equations stiff (Jain 1984), a time-splitting time-integration algorithm is used (Carcione and Quiroga-Goode 1996). The stiff part corresponding to the Biot mechanisms is solved analytically and the stiff part related to the squirt-flow and other viscoelastic mechanisms is solved with an A-stable Crank-Nicholson scheme. This method possesses the stability properties of implicit algorithms but the solution can be obtained explicitly. Single-phase viscoelastic seismic modelling also yields stiff differential equations, since relaxation peaks are not, generally, in the source frequency band. In this case, the solution is obtained with the Crank-Nicholson technique.

Let us consider the central differences and mean value operators

$$D^j\xi = \frac{\xi^{n+j} - \xi^{n-j}}{2jdt} \quad \text{and} \quad A^j\xi = \frac{\xi^{n+j} + \xi^{n-j}}{2}, \tag{A1}$$

where dt is the time step and $j=1$ or $j=1/2$.

In the Crank-Nicholson scheme, particle velocities and memory variables at time $(n+1/2)dt$ and stresses at time $(n+1)dt$ are computed explicitly from particle velocities and memory variables at time $(n-1/2)dt$ and stresses at time ndt and $(n-1)dt$. Consider, for instance, the porous differential equations (12)–(20). We proceed as follows:

1 Solve analytically the stiff part of (12)–(15) and obtain the particle velocities at time $(n+1/2)dt$ (see Carcione 1996).

2 Compute the spatial derivatives of the stresses at time ndt and then the particle velocities at time $(n+1/2)dt$ from the non-stiff parts of (12)–(15) by using the central difference operator $D^{1/2}$. Add the previous analytical solutions.

3 Compute the particle velocities at time ndt by using the mean value operator $A^{1/2}$ and then the corresponding spatial derivatives.

4 Compute ϵ from equation (5), the memory variables at time $(n+1/2)dt$ from (20) and then their mean values at ndt.

5 Compute the stresses at $(n+1/2)dt$ from (16)–(19) by using the central difference operator D^1.

The algorithms are 2nd-order accurate in time and 'infinite' (spectral) in space. The differential equations corresponding to the memory variables require an A-stable (implicit) algorithm. In the absence of viscoelastic relaxations or when the corresponding relaxation peaks are located in the source frequency band, the porous differential equations are solved with the splitting technique and an explicit 4th-order Runge-Kutta algorithm. More details are given by Carcione and Quiroga-Goode (1996).

References

Biot M.A. 1962. Mechanics of deformation and acoustic propagation in porous media. *Journal of Applied Physics* **33**, 1482–1498.

Biot M.A. and Willis D.G. 1957. The elastic coefficients of the theory of consolidation. *Journal of Applied Mechanics* **24**, 594–601.

Carcione J.M. 1995. Constitutive model and wave equations for linear, viscoelastic, anisotropic media. *Geophysics* **60**, 537–548.

Carcione J.M. 1996. Wave propagation in anisotropic, saturated porous media: plane wave theory and numerical simulation. *Journal of the Acoustical Society of America* **99**(5), 2655–2666.

Carcione J.M. and Quiroga-Goode G. 1995. Some aspects of the physics and numerical modeling of Biot compressional waves. *Journal of Computational Acoustics* **3**, 261–280.

Carcione J.M. and Quiroga-Goode G. 1996. Full frequency range transient solution for compressional waves in a fluid-saturated viscoelastic porous medium. *Geophysical Prospecting* **44**, 99–129.

Dutta N.C. and Ode H. 1983. Seismic reflections from a gas–water contact. *Geophysics* **48**, 148–162.

Dvorkin J., Nolen-Hoeksema R. and Nur A. 1994. The squirt-flow mechanism: Macroscopic description. *Geophysics* **59**, 428–438.

Gist G.A. 1994. Fluid effects on velocity and attenuation in sandstones. *Journal of the Acoustical Society of America* **96**, 1158–1173.

Gurevich B. 1996. On: "Wave propagation in heterogeneous, porous media: A velocity-stress, finite-difference method" by Dai, Vafidis and Kanasewich (*Geophysics* **60**, 327–340). *Geophysics* **61**, 1230–1232.

Gurevich B. and Lopatnikov S.L. 1995. Velocity and attenuation of elastic waves in finely layered porous rocks. *Geophysical Journal International* **121**, 933–947.

Jain M.K. 1984. *Numerical Solutions of Partial Differential Equations*. Wiley Eastern Ltd.

Kommedal J.H., Barkved O.I. and Thomsen L. 1997. Acquisition of 4-component OBS data—A case study from the Valhall field. 59th EAGE meeting, Geneva, Expanded Abstracts, B047.

Norris A.N. 1993. Low-frequency dispersion and attenuation in partially saturated rocks. *Journal of the Acoustical Society of America* **94**, 359–370.

Turgut A. and Yamamoto T. 1988. Synthetic seismograms for marine sediments and determination of porosity and permeability. *Geophysics* **53**, 1056–1067.